

Fusing in-vitro and in-vivo intravascular ultrasound data for plaque characterization

Francesco Ciompi · Oriol Pujol · Carlo Gatta ·
Oriol Rodríguez-Leor · Josepa Mauri-Ferré ·
Petia Radeva

Received: 5 February 2009 / Accepted: 5 November 2009
© Springer Science+Business Media, B.V. 2009

Abstract Accurate detection of in-vivo vulnerable plaque in coronary arteries is still an open problem. Recent studies show that it is highly related to tissue structure and composition. Intravascular Ultrasound (IVUS) is a powerful imaging technique that gives a detailed cross-sectional image of the vessel, allowing to explore arteries morphology. IVUS data validation is usually performed by comparing post-mortem (in-vitro) IVUS data and corresponding histological analysis of the tissue. The main drawback of this method is the few number of available case studies and validated data due to the complex procedure of histological analysis of the tissue. On the other hand, IVUS data from in-vivo cases is easy to obtain but it can not be histologically validated. In this work, we propose to enhance the in-vitro training data set by selectively including examples from in-vivo plaques. For this purpose, a *Sequential Floating Forward*

Selection method is reformulated in the context of plaque characterization. The enhanced classifier performance is validated on in-vitro data set, yielding an overall accuracy of 91.59% in discriminating among *fibrotic*, *lipidic* and *calcified* plaques, while reducing the gap between in-vivo and in-vitro data analysis. Experimental results suggest that the obtained classifier could be properly applied on in-vivo plaque characterization and also demonstrate that the common hypothesis of assuming the difference between in-vivo and in-vitro as negligible is incorrect.

Keywords Intravascular ultrasound · Plaque characterization · Radio frequency analysis · Sequential floating forward selection

Introduction

A vulnerable plaque is an atherosclerotic plaque that is likely to rupture or fissure, leading to thrombosis, and then to acute coronary syndrome: myocardial infarction, unstable angina pectoris, or sudden cardiac death [1–6]. The histology of atherosclerotic plaque is generally comprised of a stack of layers of cholesterol debris, calcium, and fibrous tissue. An accurate analysis of in-vivo plaque composition is an important task in diagnosis and detection of vulnerable atheroma before plaque rupture.

F. Ciompi · O. Pujol · P. Radeva
Department Matemàtica Aplicada i Anàlisi, Universitat de
Barcelona, Gran Via de les Corts Catalanes 585, 08007
Barcelona, Spain

F. Ciompi (✉) · O. Pujol · C. Gatta · P. Radeva
Computer Vision Center, Edifici O, Campus UAB, 08193
Bellaterra, Barcelona, Spain
e-mail: fciompi@maia.ub.es

O. Rodríguez-Leor · J. Mauri-Ferré
Hospital Universitari “Germans Trias i Pujol”, Carretera
de Canyet s/n, 08916 Badalona, Spain

IVUS is a powerful imaging technique that gives a detailed cross-sectional image of the vessel. It allows to explore both coronary arteries morphology and composition, thus representing an important image-guided tool for percutaneous coronary interventions.

Several IVUS-based approaches for the automatic assessment of plaque composition have been proposed, mainly based on image texture analysis [7–9] as well as processing the raw Radio Frequency (RF) signals [10–15]. Some approaches use AutoRegressive Models (ARM) [10–12] or the FFT analysis [13, 15] to compute the *power spectrum* from which spectral features are extracted, while others perform a direct measure of the *Acoustic Impedance* by Plane Wave Born Approximation [14]. Finally, approaches using the *Integrated Backscatter* parameter as discriminative feature [16–18] as well as the IVUS *Elastography* result [19–21] or the *Wavelet coefficients* [22] have been also proposed.

One of the critical issues in automatic plaque characterization problems is the creation of a reliable data *ground truth*, necessary to correctly train classifiers and to validate methods. The reliable correspondence between an atherosclerotic plaque and IVUS data can be obtained only by histological analysis of post-mortem coronary arteries. Unfortunately this methodology suffers from the complicated procedure of obtaining in-vitro data: scarce arteries availability, frequent tissue spoiling during analysis and the difficulty in finding the right correspondence between IVUS and histological image. On the other hand, obtaining data from in-vivo IVUS cases is a relatively easy task, but the obtained information can not be histologically validated. Plaques labelling in this case is performed by expert interventionists only relying on their professional experience.

The majority of plaque characterization methods presented in last years use the in-vitro data set to both train and validate the resulting classifier. The achieved overall accuracy is then solely related to the discrimination of in-vitro plaques, while it is usually assumed as the discriminative power on in-vivo data as well. This erroneous assumption is implicitly based on the hypothesis that differences between in-vivo and in-vitro IVUS data are negligible.

It is known that the presence of *blood* in in-vivo cases may modify the ultrasound echo with respect to in-vitro cases. Furthermore, even though the protocol

of in-vitro data acquisition aims to reproduce the in-vivo conditions as much as possible (for example by filling the post-mortem artery with blood [13, 15]), it is impossible to exactly reproduce the morphological and mechanical properties of an in-vivo artery. Hence, data from these two acquisition modalities can not be considered as perfectly comparable.

Nevertheless, our hypothesis is that they could share areas in the feature space, and that the inclusion of in-vivo data, after a proper selection process, could enhance the validated in-vitro data set generalizing the separation among classes. The main idea consists in keeping the in-vitro validated data set as a seed in the feature space and enhance its distribution by feeding it with a selected set of in-vivo data. The resulting *enhanced* data set is used to train a classifier that is expected to both exhibit the same (compared with the classifier trained with the initial in-vitro data set) or even better discriminative power on the in-vitro validation set and hopefully to provide more accurate plaque classification on in-vivo cases as well. The latter property can not be numerically validated since it is impossible to get a ground truth of in-vivo tissue by histological analysis, although a *qualitative* measure on the discriminative power of the enhanced classifier on in-vivo data can be assessed.

Given the differences in both acquisition modality and validation of in-vitro and in-vivo data, it is impossible to treat the data fusion process as a pure *supervised learning* problem. Since we want to keep the in-vitro data distribution as a seed for the definition of the enhanced data set, an *unsupervised* approach is not suitable. Hence, the data fusion process must be treated as a *semi-supervised* learning problem or as a supervised approach in which a *data selection process* is strictly required.

The data fusion process proposed in this work is based on a reformulated version of the *Sequential Floating Forward Selection* (SFFS) algorithm [23], regulated by a classification performance function J , in the context of plaque characterization (named *pSFFS*), and results are evaluated by *Leave-One-Patient-Out* (LOPO) [24] cross validation technique. Since we want to discriminate among *fibrotic*, *lipidic* and *calcified* tissues, the multi-class classification problem is solved by adopting the *Error Correcting Output Code* (ECOC) technique [25, 26] using AdaBoost [27] with Decision Stumps as weak classifier.

In this work we process the raw RF signal to perform spectral analysis as well as textural analysis on IVUS reconstructed images. Automatic texture analysis is usually hindered by uncontrolled IVUS data acquisition with different imaging system parameters. The image reconstruction process, performed according to a unique set of imaging parameters, gives us the chance to extract a normalized set of textural features. Both spectral and textural features are then combined in a single feature vector, providing a spectral and spatial description of the tissue.

Therefore, the main contributions of this paper are: (1) investigate the use of the SFFS algorithm as a general methodology for fusing in-vivo and in-vitro IVUS data (*pSFFS*); (2) propose and evaluate a problem specific function J such that *pSFFS* algorithm provides a final solution that is a trade-off between sensitivities while increasing the global accuracy; (3) exploit the RF data as well as reproduce the whole process of image formation in order to obtain a normalized set of IVUS features for plaque characterization. It is worth to note that the main goal of the paper is to propose a reliable data fusion strategy while not to present an exhaustive plaque characterization methodology¹.

The paper layout is as follows: section “Plaque characterization methodology” discusses the plaque characterization in in-vivo and in-vitro data: data processing, feature extraction and classification. Section “Fusing in-vitro and in-vivo IVUS data” presents the novel data fusion method and its main properties. Section “Experimental results” reports experimental results in applying the proposed method, from data acquisition to performance measurements, comprising a comparison with other plausible data fusion approaches. Discussions and conclusions end the paper.

Plaque characterization methodology

The goal of this work is to develop a technique to fuse in-vivo and in-vitro IVUS data. The main strategy consists in acquiring and processing raw

Radio Frequency data from the IVUS equipment in both in-vivo and in-vitro cases in order to extract features. Data corresponding to labelled plaques are then used as input for the *pSFFS* enhancing process, consisting of a data selection module and a classifier, for performance measurement. Figure 1 shows the pipeline of the entire procedure. For the sake of clarity, next sections give a brief description of the blocks involved in the data processing, feature extraction and classification. The *pSFFS* algorithm will be described in details in section “Fusing in-vitro and in-vivo IVUS data”.

Data processing and features extraction

IVUS RF data (acquired by either in-vivo or in-vitro cases) are processed to extract textural (from reconstructed images) and spectral (from power spectrum) features. Figure 2 schematizes the process from data acquisition to features extraction, including IVUS image formation and power spectrum computation.

Image textural features

Since the amplitude of the ultrasound echo is attenuated by its propagation through the tissue, the very first signal processing step consists in applying a *Time Gain Compensation* (TGC) function to compensate the echo signal amplitude attenuation [24]. After TGC, the IVUS image formation process comprises the following tasks (see Fig. 2):

- **Band pass filtering:** a *Butterworth* Band Pass (BP) filter of order 10 and frequencies $f_L = 20$ MHz, $f_H = 60$ MHz
- **Envelope recovering:** computed as the absolute value of the *Hilbert transform* of the RF signal
- **Logarithmic compression:** it improves the visualization of areas with a low signal intensity, as in [24, 28]
- **Digital Development Process:** a non-linear radial adjustment of the gain and edge-emphasis process to enhance the tissue visualization [9, 24]

At the end of this process, a polar representation of an IVUS image is obtained (Fig. 3a). Then, we extract a wide set of textural features by applying texture descriptors to the obtained image. As in [9] we apply a bank of 16 Gabor filters [29] and three configurations of Local Binary Patterns [30], thus

¹ The use of the proposed technique on an in-vitro data set comprising the *necrotic core* tissue is a straightforward step that is expected not to change the overall behavior and performance of the proposed framework.

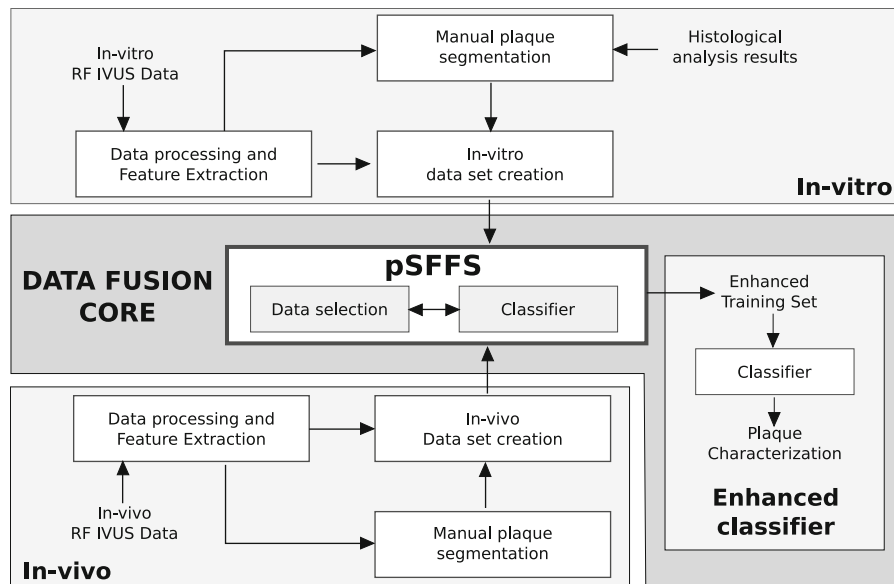


Fig. 1 Schema of the plaque characterization framework. The in-vitro and in-vivo blocks represent the IVUS data acquisition and processing task. The *pSFFS* block represents the data fusion algorithm, including a task for in-vivo data selection and

a classifier that evaluates the classification performance at each step, regulating the inclusion process. The resulting enhanced data set is then used to train an *Enhanced classifier* for plaque characterization

obtaining 19 textural features. Furthermore, due to the high echo-reflectivity property of calcified tissue, we decided to add two features, called (1) *shadow* and (2) *relative shadow*, computed by (1) accumulating the mean grey level value along each radial direction and by (2) multiplying the obtained value by the radial depth in each considered position. Finally, a 21 elements textural feature vector is obtained.

Spectral features

IVUS data power spectrum is obtained by using *AutoRegressive Model* [10, 12] (order 10, as suggested in [11]) on the TGC-compensated RF signal. The power spectrum corresponding to polar coordinates (ρ, θ) is computed by a sliding window as in [8, 11]. We take into account only the spectral information in the frequency band $B \in [f_L, f_H]$ ($f_L = 30$ MHz, $f_H = 50$ MHz), centered in the working frequency of the transducer, $f_0 = 40$ MHz. With the aim of extracting compact spectral features, we characterize the power spectra using two straight lines: being $S(f)$ the power spectrum function and defining $f_M = \arg \max_{f \in B} S(f)$, we compute the straight lines fitting the curves $S^+ = S(f)|_{f \in [f_L, f_M]}$ and $S^- = S(f)|_{f \in [f_M, f_H]}$. The

spectral feature vector is then composed by the two straight line *slopes*, *y-axis-intercept* values, $S(f_M)$, $S(f_L)$, $S(f_H)$, $S(0)$ values, the *energy of A-line* and finally, the *averaged amplitude of spectral component* in B .

The final feature vector is constructed by concatenating image textural and spectral features (see Fig. 2) with the aim of blending the appearance of the tissues with information obtained from their spectral content. It is our belief that image-based and RF signal analysis provide complementary data for the accurate description of tissue composition and leads to a rich set of features to be selected and weighted by the classifier.

Plaque classification

The proposed *pSFFS* methodology needs the definition of a proper classifier. It has been shown that, for plaque classification, AdaBoost [27] with Decision Stumps exhibits high performance in terms of accuracy and efficiency [8]. Since we want to discriminate among *fibrotic*, *lipidic* and *calcified* tissue, a multi-class problem arises. ECOC [25, 26] is an effective technique to solve multi class problem by decomposing them into a set of binary problems [31].

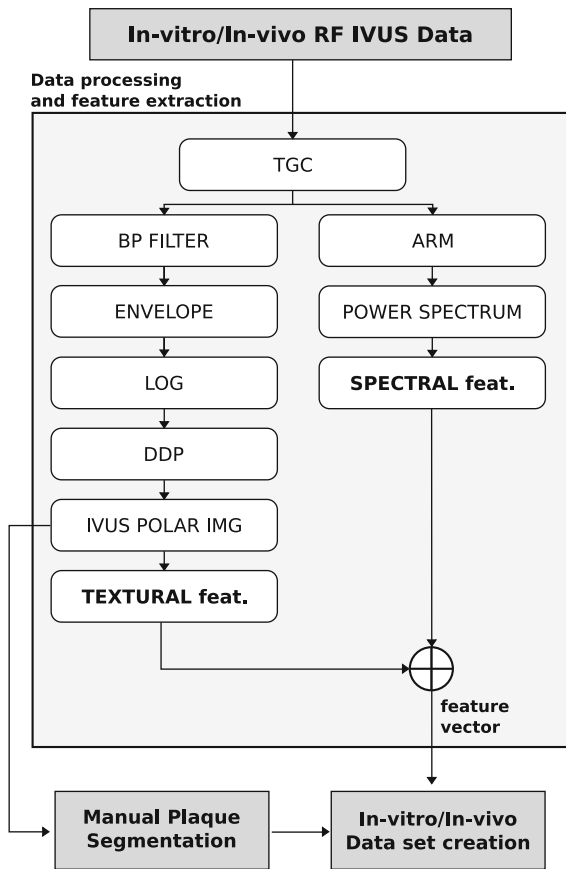


Fig. 2 Detailed schema of the *Data processing and Feature Extraction* block of Fig. 1. From the TGC-compensated RF signal, both the IVUS polar image and the power spectrum are computed, hence textural and spectral features are extracted

The ECOC framework is independent from the used classifier, thus allowing to combine several binary classifiers (discriminative or generative), to jointly classify an unknown example. Given the number of classes C and a *coding* strategy, K binary classifiers are trained and an ECOC matrix $\mathbf{M} \in \{-1, 0, +1\}^{C \times K}$ is designed. Each column in the ECOC matrix corresponds to a binary classifier while each row represents a class codeword; a zero value in a certain position of \mathbf{M} means that we do not care about the classification result for that particular class and problem. Given an unknown example and a *decoding* distance measure, a codeword $w \in \{-1, 1\}^{1 \times K}$ is obtained and its distance with each row of \mathbf{M} is computed. The inferred class corresponds to the minimum distance row.

This inference technique implicitly embeds an error-correction property, characteristic of the ECOC framework. Furthermore, it is possible to demonstrate that other multi-class extension approach (e.g., the *major voting* technique) are special cases of ECOC, obtained by choosing a particular coding and decoding strategy. In this work we use *one-vs-one* coding and *Attenuated Euclidean Distance* (AED) [32] decoding strategy.

Fusing in-vitro and in-vivo IVUS data

As discussed above, we propose to use in-vivo data to enhance the in-vitro data set. Our approach is based

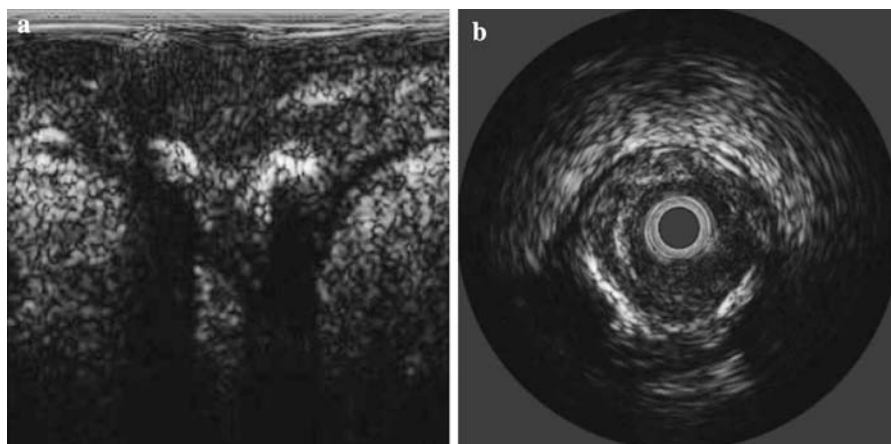


Fig. 3 **a** In-vivo IVUS image in polar coordinates and **b** in cartesian coordinates, representing the *cross-sectional* IVUS image

on iterative and controlled inclusion of in-vitro plaques into the in-vitro training set according to a selection criterion based on the value of a classification performance parameter evaluated while discriminating in-vitro tissue.

Sequential Floating Forward Selection has been proposed in [23] as a features selection algorithm, based on inclusion and conditional exclusion of data. For our purposes, we consider that an IVUS *frame* can contain different plaques which we consider as a monolithic block of information, i.e., all the plaques in a frame can be included or removed from the data set but partial inclusion/exclusion of a specific class example (e.g., removing the *calcified* and keeping the *fibrotic* plaque) is not allowed. This approach is justified by the idea that the inter-patient differences in appearance of plaques will be preserved if the information of a single frame is treated as monolithic; furthermore, the over-fitting phenomenon of the classifier on a specific set of examples is potentially avoided.

Since the inclusion criterion actually consists in evaluating a classification performance parameter while including data, a proper definition of the *training/testing* process represents a key part of the

algorithm. Let us define $p = 1, \dots, N_p$ the index of in-vitro cases. In order to define the data sets to use in the data fusion algorithm, the in-vitro data set is split into three parts (Fig. 4): the first part, called X^p , is obtained by removing the p th necro case from the whole data set and it is used in the selection process, thus representing the *training* data set, while the second part, called X_{val}^p is not used during the selection process and represents the *validation* data set. The third part, extracted from X^p , is related to the data inclusion process and is defined below.

The parameter that controls the data selection process in the *pSFFS* is called J and it is actually a value that depends on the result of a classification step. In our approach, the classification is performed on in-vitro data, being the only reliable data set to use while looking for an improvement in tissue discrimination. In order to produce stable and reliable classification results, a cross validation technique must be used. The J parameter is then a function of the classification performance, computed according to the defined cross validation process.

Once the cross validation technique is defined, the third part of the data set is then obtained as a subset of the X^p in-vitro *training* data set and represents the *test*

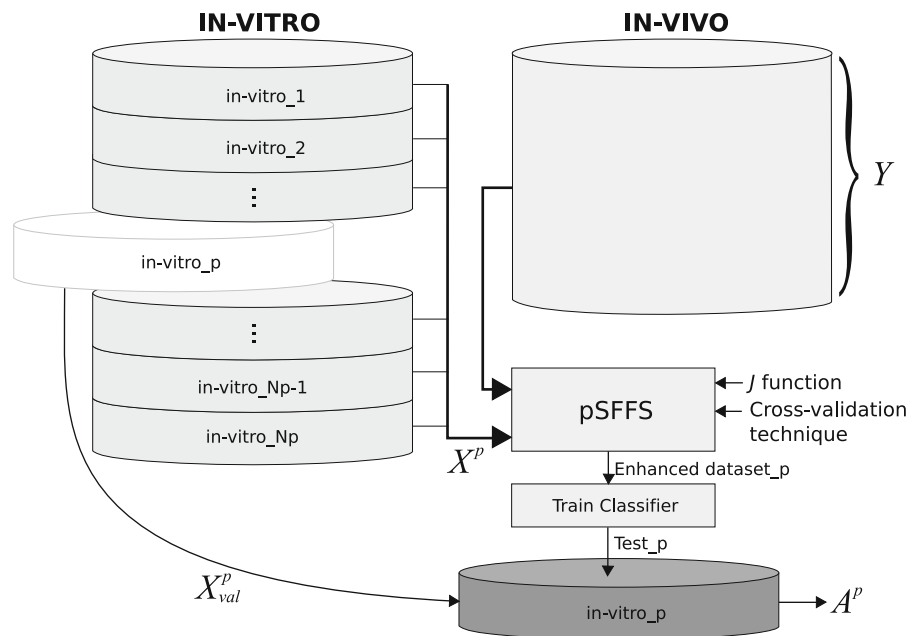


Fig. 4 Detailed description of the *data fusion core* (see Fig. 1). According to the Leave-One-Patient-Out technique, the in-vitro data set is used in both the data fusion process and

in validating the discriminative power of the enhanced classifier, while the in-vivo data is solely involved into the data fusion process

Algorithm 1 Function $\widehat{CP} = CP(X^p, \bar{Y}, f_{cv})$

Require: X^p {The *in-vitro* training set}

Require: \bar{Y} {The *in-vivo* data set}

Require: f_{cv} {The cross validation function}

Ensure: \widehat{CP} {A classification performance parameter}

- 1: define N {number of folds required by the cross validation technique}
- 2: initialize $CP[N] = 0$ { N -elements empty vector}
- 3: **for** $i = 1:N$ **do**
- 4: define $x_i \subset X^p$ {test set}
- 5: define $TRAIN_i = \{X^p \setminus x_i\} \cup \bar{Y}$
- 6: define $TEST_i = x_i$
- 7: $classifier = training(TRAIN_i)$ {train}
- 8: $CP[i] = classifier(TEST_i)$ {test}
- 9: **end for**
- 10: $\widehat{CP} = mean(CP) \pm std(CP)$

data. It is used, during the *in-vivo* data selection process, to assess the classification performance at each iteration k of the process. Before illustrating the *pSFFS* algorithm, it is worth to define the cross validation procedure used to obtain the classification performance parameters necessary to compute the value of J . Let us call f_{cv} the chosen cross validation function, \bar{Y} a generic set (or subset) of *in-vivo* data and \widehat{CP} a generic classification parameter (for example $\widehat{CP} = overall\ accuracy$). The classification performance are then obtained as depicted² in Algorithm 1. Finally, the J value is computed as $J(\widehat{CP})$. The formulation and properties of J will be explained in section “Design of J function”. As suggested in [33], the 5-fold cross validation is used as appropriate during the data selection process. At each fold, the total amount of *in-vivo* data involved into the inclusion process is limited to the 30% of the *in-vitro* data set length, while the size of X^p has been set to 6,000 points by random subsampling of data. Hence, with a 5-fold cross validation, the test set consists in 1,200 points.

We formulate now the data selection process of the *pSFFS* algorithm for the creation of the enhanced data set. Since we are mainly interested in the discriminative property of the enhanced classifier while classifying *in-vitro* cases, we will evaluate its discriminative power by a Leave-One-Patient-Out cross validation technique [24]. According to this procedure, given the number N_p of *in-vitro* cases, the

creation of the enhanced data set is repeated N_p times, and then validated by testing the enhanced classifier on X_{val}^p , thus providing the validation results as the average over N_p classification performance values. For the sake of clarity, the fusion problem is now formulated with respect to an individual fold of the LOPO technique, i.e., when the generic p th *in-vitro* case is left out, as follows.

Let us call X the initial *training* set composed of frames from *in-vitro* (actually X_p) and Y the set of frames of *in-vivo* cases. The *pSFFS* requires the definition of a function of the classifier performance J , that controls the inclusion-exclusion process, and also a cross validation technique to use while computing J . When both initial data and the required functions are defined, the *pSFFS* method can be formulated (see Algorithm 2). The algorithm alternates two phases: an *inclusion* loop (lines 12–19) and a *conditional exclusion* of one frame (lines 24–30). The condition to include one frame is that the training/test process by cross validation produces a score J that is greater than before (lines 12–13); with the same rule, the exclusion step can remove one of the frames already included in the set if this increases J (lines 24–25). If during the conditional exclusion none of the candidate frames increases J , the algorithm checks the number of times the J value decreased (line 34). In the case J decreased too many time, actually more than d_M times, the algorithm stops, otherwise the algorithm admits an *unconditional inclusion* and updates d value. This stop procrastination procedure is necessary to avoid stopping the algorithm at the first maximum value since it can be suboptimal. In each case, the optimal set is stored (lines 17,29), in order to obtain the best achievable classification performance. Hence, at the end of the selection process, the enhanced data set consists in X_{EN} , i.e., the combination of *in-vitro/in-vivo* data obtained in correspondence of $J_{max} = J(X, Y_{EN})$.

Design of J function

The whole *pSFFS* is regulated by the function J , thus its definition is critical for the algorithm performance. As stated above, the value of J depends on one or more classification performance parameter. In previous section the computation of such generic parameters has been explained. In this section we want to define the analytical formulation of the parameter J as a function of classification performance parameter.

² The function is described in pseudo-Matlab code.

Algorithm 2 pSFFS

Require: X {The set of *in-vitro* frames}
Require: Y {The set of *in-vivo* frames}
Require: J {The J function definition}
Require: f_{cv} {The cross validation function}
Ensure: X_{EN} {The enhanced (fused) data set}

1: Note: to simplify the formulation, $J(CP(X, Y, f_{cv})) = J(X, Y)$
2: $k = 0$
3: $d = 0$
4: set d_M
5: $X_0 = X$
6: $Y_T = \emptyset$
7: $X_{EN} = X$
8: STOP = *false*
9: INCLUDE = *true*
10: **while** !STOP **do**
11: **if** INCLUDE **then**
12: $y^+ = \arg \max_{y \in Y} J(X, Y_T \cup y)$
13: **if** $J(X, Y_T \cup y^+) > J(X, Y_T)$ **then**
14: $Y_T = Y_T \cup y^+$
15: $k = k + 1$
16: $X_k = X \cup Y_T$
17: $X_{EN} = X \cup Y_T$
18: $Y_{EN} = Y_T$
19: $Y = Y \setminus y^+$
20: **else**
21: INCLUDE = *false*
22: **end if**
23: **else**
24: $y^- = \arg \max_{y \in Y_T} J(X, Y_T \setminus y)$
25: **if** $J(X, Y_T \setminus y^-) > J(X, Y_T)$ **then**
26: $Y_T = Y_T \setminus y^-$
27: $k = k + 1$
28: $X_k = X \cup Y_T$
29: $X_{EN} = X \cup Y_T$
30: $Y_{EN} = Y_T$
31: INCLUDE = *true*
32: **else**
33: $d = d + 1$ {Increase the number of time J
 decreased}
34: **if** $d > d_M$ **then**
35: STOP = *true*
36: **else**
37: $y^+ = \arg \max_{y \in Y} J(X, Y_T \cup y)$
38: $Y_T = Y_T \cup y^+$
39: $k = k + 1$

Algorithm 2 continued

40: $X_k = X \cup Y_T$
41: $Y = Y \setminus y^+$
42: **end if**
43: **end if**
44: **end if**
45: **end while**

For this reason, in the rest of the paper, we will refer to the J parameter as the *function* J .

Given a generic classification results, the *sensitivity* (S) parameter can be defined as

$$S = \frac{TP}{TP + FN},$$

where TP indicates the *true positives* and FN the *false negatives*. In the proposed plaque characterization problem, it is clear that a high sensitivity in classifying the test set assures that validated plaques are classified as such. Hence, the mean sensitivity, together with the overall accuracy

$$A = \frac{TP + TN}{TP + TN + FP + FN},$$

where TN indicates the *true negatives* and FP the *false positives*, are the parameters to maximize. For this reason, we define J as a weighted linear combination of the *weighted averaged sensitivity* over all the classes and the *overall accuracy* as

$$J_k = \alpha \underbrace{\sum_{l=1}^{N_c} w_k^l S_k^l}_{j^s} + (1 - \alpha) A_k, \quad (1)$$

where S_k^l and w_k^l are the *sensitivity* and the *weighting* for the class l at algorithm iteration k , respectively, N_c is the number of classes, A_k is the overall accuracy and $\alpha \in [0, 1]$ is a coefficient that regulates the importance of each term. To avoid the algorithm to increase the sensitivity of a class at the cost of an excessive reduction of other classes sensitivity, w_k^l is dynamically defined to be inversely proportional to the class *sensitivity* itself:

$$w_k^l = \frac{\log\left(\frac{1}{S_k^l}\right)}{\sum_{l=1}^{N_c} \log\left(\frac{1}{S_k^l}\right)} \quad (2)$$

During iteration k , if one of the classes has a *sensitivity* close to one, the corresponding weight tends to zero. For this reason, this class will poorly influence the inclusion/exclusion process letting the $pSFFS$ algorithm to search for frames that improve other classes sensitivity. We refer to the sensitivity-based term of J equation as J^S . Finally, the term proportional to the accuracy guarantees an inclusion process in which not only the sensitivities are balanced, but also the global classification performance is improved. The importance of both the sensitivity and accuracy terms is regulated by the α coefficient, experimentally set to 0.4 by cross validation.

The J^S term presents an interesting property that can be explained in a general though simplified case, analyzing a two classes classification problem. The contribution given by J^S in fact allows to obtain a trade-off between sensitivities of all plaques. This appears clearly in Fig. 5 where oriented arrows show the gradient direction and curves are the level-sets of J^S as a function of the sensitivities (S^1 and S^2) of two generic classes. The gradient vector field can be seen as positive linear combination of one vector field that points toward the loci where $S^1 = S^2$, thus searching for a sensitivities trade-off (avoiding for instance $S^1 \rightarrow 1$ and $S^2 \rightarrow 0$), and another vector field that points towards $S^1 = S^2 = 1$, trying to maximize sensitivities.

Experimental results

The IVUS equipment used in this work is a *Galaxy II IVUS Imaging System* (Boston Scientific) with a catheter *Atlantis SR Pro 40 MHz* (Boston Scientific), installed in the Hospital “*Germanys Trias i Pujol*” of Badalona (Spain). RF data are collected using a 12-bit acquisition card ($f_s = 200$ MHz) and stored as frames of 256 A-lines by 1,024 samples each one.

Data acquisition

In-vivo data are acquired during a normal hemodynamic intervention procedure. Once the intervention is over, an *IVUS pullback* is acquired by storing data while the probe is *pulled-back* at constant speed³. The

³ The catheter is connected to the IVUS equipment by a motorized tool and its position is constantly monitored by X-ray analysis.

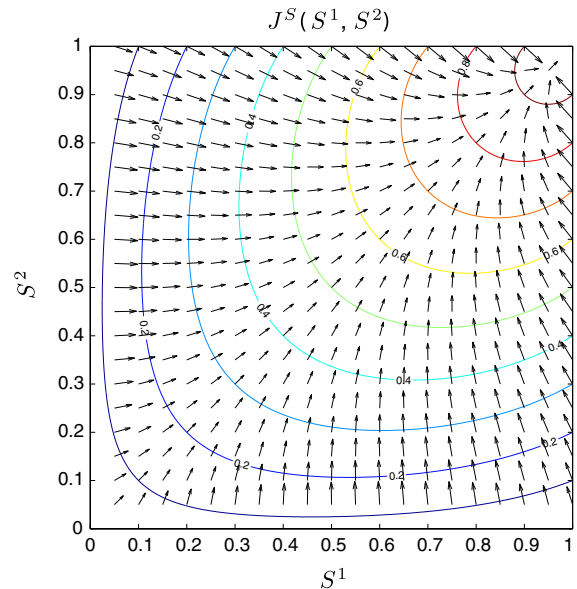


Fig. 5 Level-sets (continuous curves) and gradient (arrows) of J^S as a function of sensitivities S^1 and S^2

result is a sequence of images describing the cross sectional vessel structure. *In-vivo* data have been collected from nine patients, plaques have been labelled by two experts resulting in 76 frames, containing 49 *fibrotic*, 37 *lipidic* and 35 *calcified* plaques. To improve the labelling reliability, we rejected the labelling where the two experts were in blind disagreement.

In-vitro data are acquired from post-mortem cases. The artery, separated from the heart, is first fixed on a mid-soft plane (Fig. 6a) and filled (using a catheter) with physiological saline solution at constant pressure (around 120 mmHg), simulating blood pressure. The distal and proximal, together with left and right hand positions are marked in the panel to be used as a reference. The probe is then introduced through the catheter and RF data are acquired in correspondence of plaques. These positions are clearly marked on the external part of the artery. The vessel is then cut in correspondence with previously marked positions and plaque composition is determined by histological analysis. For each cut, the tissue composition is observed at the microscope, and an image is then obtained (Fig. 6b). Taking into account the reference positions in the panel and the orientation of the IVUS image, it is possible to establish a correspondence between the plaques detected by histology and their respective areas in the IVUS image (Fig. 6c). This

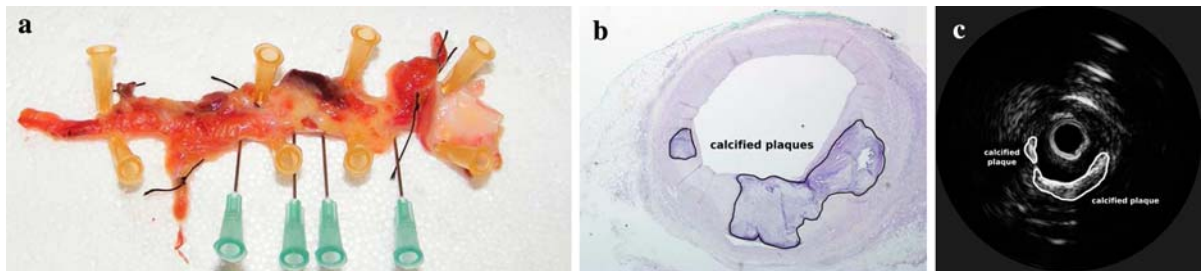


Fig. 6 Set up for IVUS acquisition from post-mortem artery. **a** coronary artery, fixed on the plane with marked positions clearly shown; **b** plaque segmentation on histological image and **c** corresponding segmentation on reconstructed IVUS image

task is assigned to experts interventionists in cooperation with pathologists.

The different conditions and modalities in which the two images are acquired are profoundly different. The mechanical consistence given to the artery while acquiring IVUS data is impossible to be exactly maintained when the vessel is sectioned and analyzed. Phenomena of tissue spoiling and a certain error in finding the exact correspondence between the IVUS and the histological image make hard to get an exact registration and, consequently, a reliable automatic labelling. For these reasons, we follow a protocol in which the medical team manually performs the plaque labelling task, rather than using a dedicated software [11, 12], discarding pairs of images in which a reliable correspondence can not be obtained. By following this procedure, in-vitro IVUS data have been collected from nine post-mortem arteries, resulting in 50 frames with 26 *fibrotic*, 14 *lipidic* and 31 *calcified* plaques.

Validation methodology

Using the enhanced data set provided by the *pSFFS* algorithm, an AdaBoost classifier has been trained using up to 50 Decision Stumps [27]. As done before, to tackle the multi-class problem we used the ECOC framework [25, 26], devised using an *one-versus-one* coding with *AED* decoding. Classification performance is evaluated by *LOPO* cross validation technique: the enhanced training set is built by fusing selected in-vivo and all data frames from in-vitro cases, leaving out one necro case, which frames are used as a test (Fig. 4). The process is repeated for all cases and a confusion matrix is computed at each round. The classification results are evaluated at each one of the N_p fold, and the whole process is repeated

for $N_r = 20$ rounds, in order to get more robust results. At each round we evaluate the *overall accuracy* (A), the *sensitivity* (S), the *specificity* (K) and the *positive predictive value* (*precision*) (P) for each class, then the mean value and standard deviation of the N_r performance parameters are computed.

Algorithm evaluation

The proposed method is validated by considering classification parameters as described in the previous section. Figure 7 shows the evolution of the J parameter, up to the 12th iteration (where the optimal set X_{EN} is found) for a generic p th case of the analysis. The depicted J value is the one obtained during the data selection process, while the values of accuracy and sensitivity are obtained by testing on the p th necro case (X_{val}^p), left out during the data selection process. It is worth to note that, while J increases (during data selection), the performance parameters when testing on an unknown case increase as well, though with a different profile. This phenomenon is expected since the train/test data set may not be perfectly representative of all the possible cases, thus the enhanced data set $X_{EN} = X \cup Y_{EN} : J(X, Y_{EN}) = J_{max}$ may not produce the A_{max} while validating on a real case. Nevertheless, in our experiments we always get $A(X_{EN}) > A(X_0)$ in the validation step: this means that the characterization accuracy while characterizing in-vitro cases with a classifier trained with the X_{EN} training set is always higher than the accuracy obtained with a classifier trained only with in-vitro data. This result clearly demonstrates the effectiveness of the proposed approach while validating results on in-vitro data set.

Table 1 reports the classification performance parameters obtained while testing on in-vitro cases

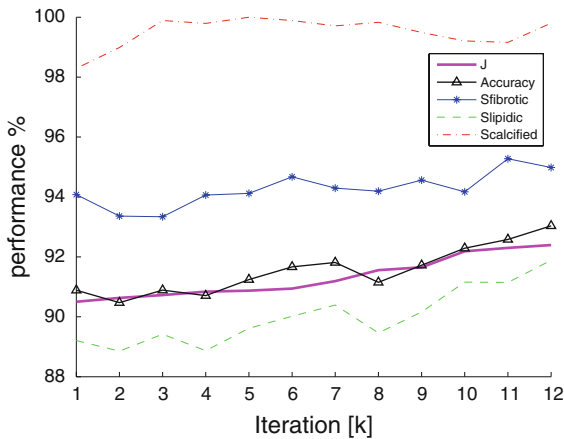


Fig. 7 Example of the *pSFFS* algorithm performance up to 12th iteration. This case is specific for a generic *p*th necro case. *J* is the value achieved at each iteration during the data selection process, while the *overall accuracy* and *sensitivity* (*S*) for each tissue type are computed by characterizing the X^p_{val} data at each iteration

Table 1 Performance as MEAN (STD) of analyzed methods on classifying in-vitro data

	<i>IvtD</i>	<i>BI</i>	<i>pSFFS</i>	<i>LDS</i>
<i>A</i>	89.93 (0.29)	89.57 (0.58)	91.59 (0.47)	84.96 (0.78)
<i>S_{fib}</i>	90.46 (0.60)	87.66 (0.85)	92.58 (0.95)	87.68 (0.95)
<i>S_{lip}</i>	80.49 (0.80)	89.61 (1.08)	85.21 (0.59)	89.87 (1.31)
<i>S_{cal}</i>	92.20 (0.46)	89.70 (0.93)	92.29 (0.75)	75.98 (2.23)
<i>K_{fib}</i>	92.16 (0.41)	91.71 (0.52)	93.85 (0.34)	85.88 (1.43)
<i>K_{lip}</i>	95.50 (0.17)	92.94 (0.88)	96.47 (0.37)	92.25 (0.92)
<i>K_{cal}</i>	96.15 (0.48)	96.37 (0.52)	96.21 (0.38)	95.64 (0.60)
<i>P_{fib}</i>	93.34 (0.33)	92.80 (0.70)	94.72 (0.30)	89.03 (1.26)
<i>P_{lip}</i>	69.48 (0.86)	74.25 (2.07)	74.78 (2.09)	65.44 (2.72)
<i>P_{cal}</i>	92.48 (0.86)	97.61 (0.37)	93.23 (0.62)	91.66 (1.64)

The *overall accuracy* (*A*), the *sensitivity* (*S*), *specificity* (*K*) and *precision* (*P*) are computed when discriminating *fibrotic* (*fib*), *lipidic* (*lip*) and *calcified* (*cal*) plaque

according to the LOPO cross validation technique described in previous section. Figure 8 shows some example of in-vitro plaque characterization performed with the classifier trained using optimal training set.

Selection: features space perspective

Our hypothesis is that data from in-vivo and in-vitro acquisition modalities could share areas in the feature

space, and that in-vivo data inclusion, after a proper selection process, could enhance the validated data set generalizing the separation among classes. To verify this hypothesis from the point of view of the feature space, we compare the data distribution of in-vivo, in-vitro, in-vivo *selected* and *enhanced* sets using the *Bhattacharyya* distance [34] as a measure of multivariate distribution closeness and overlapping. Table 2 reports *Bhattacharyya* distances among different plaques. With the aim of visualizing the inter-distance between the distributions in Table 2, we project the distances on a plane by means of the *Multidimensional Scaling* algorithm [35], obtaining Fig. 9.

It can be noted that, confirming our hypothesis, the in-vitro and in-vivo distributions for each class can be clustered in clearly separated areas. The proposed algorithm selects in-vivo examples depending on the degree of separation that their inclusion provide. Note that selected data can be highly (*calcified* tissue) or loosely (*fibrotic* and *lipidic* tissue) representative of the entire in-vivo data set. Relative projected distances among classes suggest that a classifier trained with enhanced in-vitro validated data could be used to classify in-vivo data (see Fig. 9). To corroborate this hypothesis, hypothetical 2D projection of hyperplanes bounding the enhanced data sets have been illustrated; the separation bounds have been defined by crossing the mid point of each segment connecting the projected centers of enhanced data points. In this simplified though representative case it results clear that the bounds separating the enhanced data are able to discriminate plaques in both in-vitro and in-vivo cases as well.

In order to clearly understand the relationship between in-vivo and in-vitro data, we perform a comparison of the used features in both data types. For this purpose, a set of points corresponding to each feature has been extracted from the two data set. Hence, for each feature, the *Bhattacharyya* distance has been computed between the two data examples. Since each tissue type exhibits different properties in both textural and spectral features space, this process has been separately repeated for each class (*fibrotic*, *lipidic*, *calcified* plaque). Figure 10 shows the bar diagram of the resulting normalized distances for the considered cases: features from 1 to 21 correspond to texture analysis while from 22 to 35 correspond to spectral analysis.

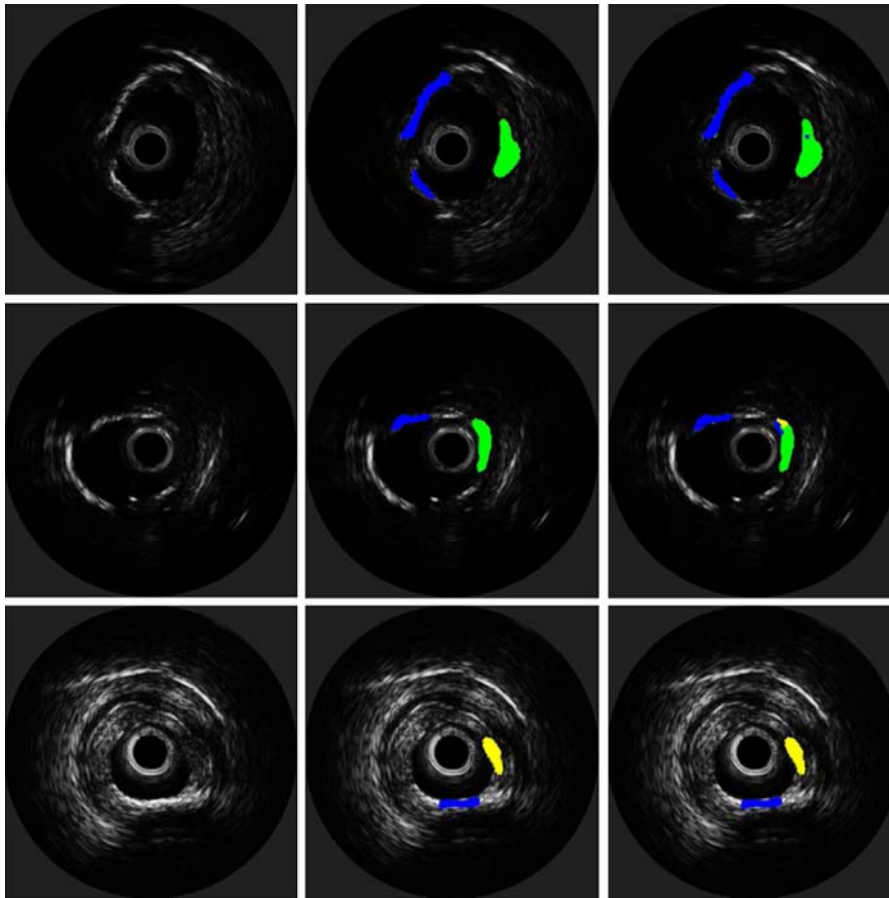


Fig. 8 Plaque characterization on IVUS data. *First column* original reconstructed IVUS images; *second column* histologically validated ground-truth plaque segmentation; *third column* classification result. *Yellow, green and blue* (corresponding to light, medium and dark grey) color indicate *lipidic, fibrotic and calcified* tissue, respectively (Color figure online)

Table 2 Bhattacharyya distances among plaques for *fibrotic (Fib)*, *lipidic (Lip)* and *calcified (Cal)* classes

	Fib_{ivt}	Lip_{ivt}	Cal_{ivt}	Fib_{ivv}	Lip_{ivv}	Cal_{ivv}	Fib_{sel}	Lip_{sel}	Cal_{sel}	Fib_{enh}	Lip_{enh}	Cal_{enh}
Fib_{ivt}	0	2.24	6.04	5.29	4.16	12.99	10.14	3.79	16.5	0.45	3.97	5.47
Lip_{ivt}	2.24	0	8.60	12.10	4.57	18.28	18.62	3.98	20.3	5.30	0	10.29
Cal_{ivt}	6.04	8.60	0	7.13	10.46	5.04	13.78	10.89	8.57	5.41	8.28	0.21
Fib_{ivv}	5.29	12.10	7.13	0	11.29	8.18	1.99	10.48	9.38	3.93	9.86	7.84
Lip_{ivv}	4.16	4.57	10.46	11.29	0	18.36	17.15	1.28	19.38	6.28	1.94	11.04
Cal_{ivv}	12.99	18.28	5.04	8.18	18.36	0	13.62	18.54	2.42	10.95	15.95	4.71
Fib_{sel}	10.14	18.62	13.78	1.99	17.15	13.62	0	19.39	15.13	5.88	14.81	12.17
Lip_{sel}	3.79	3.98	10.89	10.48	1.28	18.54	19.39	0	20.93	6.55	1.97	11.61
Cal_{sel}	16.5	20.3	8.57	9.38	19.38	2.42	15.13	20.93	0	14.53	18.04	6.69
Fib_{enh}	0.45	5.30	5.41	3.93	6.28	10.95	5.88	6.55	14.53	0	4.67	5.21
Lip_{enh}	3.97	0	8.28	9.86	1.94	15.95	14.81	1.97	18.04	4.67	0	8.60
Cal_{enh}	5.47	10.29	0.21	7.84	11.04	4.71	12.17	11.61	6.69	5.21	8.6	0

The distances are computed among the in-vitro (*ivt*), *in vivo* (*ivv*), the in-vivo *selected* data sub-set (*sel*) and the *enhanced* data set (*enh*)

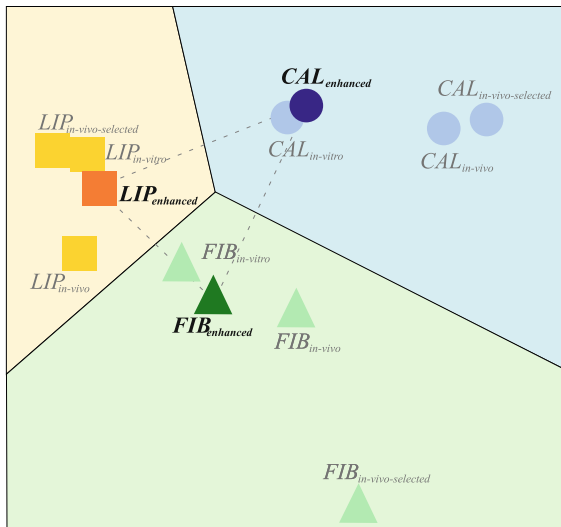


Fig. 9 Multidimensional scaling on Battacharyya distances among plaque classes. Hypothetical qualitative hyperplanes separating the enhanced data set with *one-vs-all* strategy are represented

Note that in most ($\sim 80\%$) of the cases, the distance between in-vivo and in-vitro features is low, thus confirming the initial hypothesis that they share areas in the feature space. On the other side, the presence of highly different features ($\sim 20\%$) enforces the necessity of a proper data fusion process. In particular, the features 1–3, corresponding to three configurations of Local Binary Patterns, result in a high distance in both fibrotic and calcified tissue. From this result, we can deduce that some textural properties in these two tissue types present significant differences between in-vitro and in-vivo cases. This phenomenon is not present in the lipidic class instead; this can be explained with the fact that in lipidic plaque the signal intensity is usually extremely low, thus reflecting small differences into the appreciable texture. Nevertheless, the spectral content of lipidic tissue exhibits a high distance between in-vivo and in-vitro cases.

Comparison

At the best of our knowledge, in-vivo and in-vitro IVUS data fusion is a completely novel technique. For this reason, there are no related methods that directly address this problem. Thus, we compare the proposed method with two approaches that mix different data

sets. With each one of the two approaches, the enhanced data set is created and used to train a classifier. In both cases, the discriminative power of the resulting classifier is assessed by classifying in-vitro data by LOPO cross validation. Hence, once the enhanced training set is defined, the validation process is exactly the same as the one used in *pSFFS*.

The first considered method creates a new training set by simply fusing all the available in-vivo data and in-vitro data. The labelling of the in-vivo data is used as it is, without any kind of selection. For this reason we named this naïve method as *basic inclusion* (BI), representing a pure *supervised* approach in which the labelling provided by experts is considered as completely reliable.

The second method, called *Low Density Separation* (LDS) [36] is much more complex and belongs to the *semi-supervised* learning algorithms. Based on cluster assumption, LDS trains a *Transductive Support Vector Machine* (TSVM) [37] by gradient descent on a graph-distance derived kernel. The graph is constructed by assigning to each edge a weight given by the Euclidean distance with each other feature point. The main idea is that two points in the same cluster present a continuous connecting curve passing through regions of high density, while two points of different clusters are connected with curves traversing a density valley. The similarity of two points is then defined by maximizing over all continuous connecting curves the minimum density along the connection. In LDS-based inclusion, both in-vitro and in-vivo data have been used to construct the distance graph and the TSVM has been trained. in-vivo points are added to the training set with labels provided by LDS classification results and the enhanced set is created. LDS parameters have been set as $(C, \rho, \sigma) = (850, 0.05, 0.001)$ by cross validation.

Test In-vitro

Table 1 shows the classification parameters for BI, LDS and *pSFFS* methods when characterizing in-vitro data, compared with the initial plaque characterization performance using exclusively in-vitro data (*IvtD*) as training set. In the BI, LDS and *pSFFS* cases, the classifier has been trained by using the enhanced data set obtained by applying each one of the considered methods. Note that the proposed

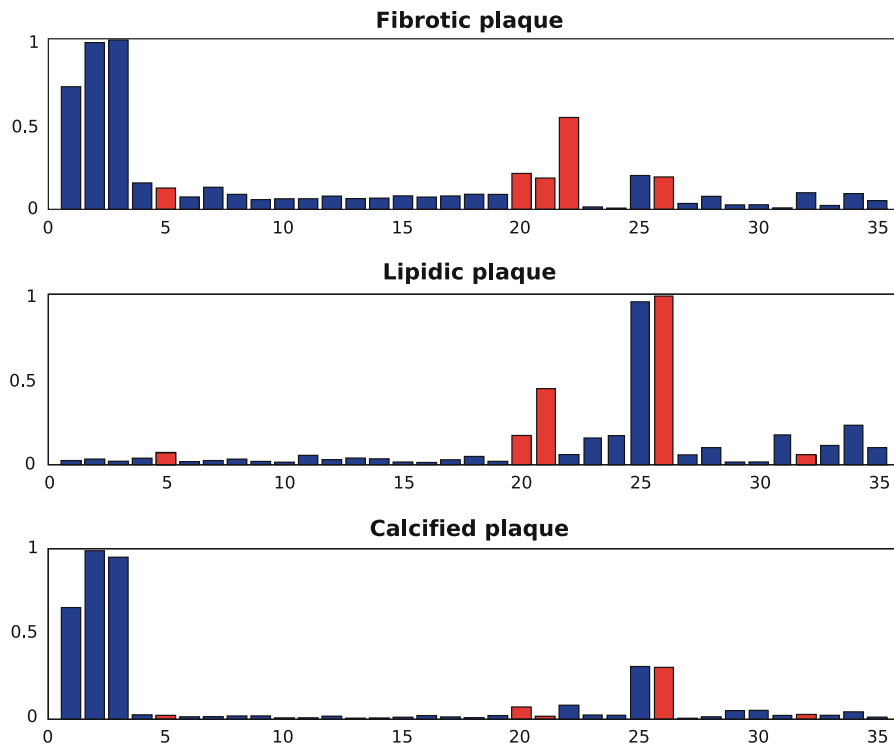


Fig. 10 Feature comparison between in-vitro and in-vivo data. The *x*-axis indicates the feature index while the *y*-axis depicts the normalized feature distance, computed by using Bhattacharyya

distance. In *red* the features that result as the most important when discriminating in-vitro data (see section “Comparison” for details) (Color figure online)

algorithm outperforms all the methods used in the comparison, providing a mean improvement in performance parameters of 1.9% respect to the *IvtD* case.

Test In-vivo

Results in Table 1 highlight that in an IVUS-based atherosclerotic plaque data fusion problem, a *supervised* approach with *data selection* is more suitable than a *semi-supervised* one.

Hence, it has been proved that the enhanced classifier performs equally, or even better, than a classifier trained and validated only on in-vitro cases. Note that the last approach has been followed by almost all the plaque characterization methods presented in the last 10 years, on the hypothesis that the differences between in-vitro and in-vivo data are negligible.

In the proposed approach, the training data set is designed by fusing in-vivo and in-vitro IVUS data. It is then reasonable to assume that the enhanced

classifier could exhibit better performance in discriminating in-vivo data with respect to a classifier trained only with in-vitro data. Note that this assumption does not imply any hypothesis on the similarity between in-vivo and in-vitro data; it is in fact naturally deduced since the enhanced data set includes examples of in-vivo data, thus providing to the classifier a knowledge about the spatial distribution of in-vivo points. In order to prove the last hypothesis, we compared the classification results of both the *IvtD* and the *pSFFS* classifiers when discriminating plaques in in-vivo cases: Table 3 shows the obtained classification performance in both cases.

Given the impossibility for obtaining the absolute knowledge on in-vivo tissue composition by histological analysis, it is clear that the obtained results can not be considered as a reliable, though *qualitative* results. Notwithstanding that, the increment of about 13% in overall accuracy when the *pSFFS* classifier is used indicates the benefits achieved in using an enhanced data set instead of a pure in-vitro training set.

Table 3 Performance as MEAN (STD) of *IvtD* vs. *pSFFS* methods in classifying in-vivo data

	<i>IvtD</i>	<i>pSFFS</i>
<i>A</i>	74.05 (1.34)	87.09 (0.33)
<i>S_{fib}</i>	88.49 (3.36)	90.66 (0.43)
<i>S_{lip}</i>	27.87 (3.50)	58.46 (1.61)
<i>S_{cal}</i>	99.62 (0.11)	99.37 (0.22)
<i>K_{fib}</i>	67.54 (1.53)	85.86 (0.55)
<i>K_{lip}</i>	97.53 (1.49)	98.56 (0.09)
<i>K_{cal}</i>	96.67 (0.26)	96.32 (0.24)
<i>P_{fib}</i>	55.90 (1.27)	73.85 (0.72)
<i>P_{lip}</i>	83.93 (7.95)	92.59 (0.33)
<i>P_{cal}</i>	94.74 (0.38)	95.82 (0.26)

The overall accuracy (*A*), the sensitivity (*S*), specificity (*K*) and precision (*P*) are computed when discriminating fibrotic (*fib*), lipidic (*lip*) and calcified (*cal*) plaque

In order to corroborate the experimental results obtained when classifying in-vivo data with both *IvtD* and the enhanced classifier, we computed the weight assigned by AdaBoost to each feature, when trained only with in-vitro data. For this purpose, the LOPO process with *one-vs-one* coding has been repeated $N = 20$ times and at each round the weight of each feature have been cumulated separately for each one of the three classes. Finally, the five most important features have been considered; the resulting discriminative features are indicated in Fig. 10. Since most of the in-vitro discriminative features exhibit a high distance value respect to in-vivo data, the low accuracy achieved when classifying in-vivo data with the *IvtD* classifier is justified. Furthermore, these results enforce the benefits achieved with the enhanced classifier.

Discussions

The proposed *pSFFS* method improves the performance parameters of all the classes on average and outperforms other approaches. The sensitivity of each class, compared with the *IvtD* case, is improved; in particular, the class starting with the lowest sensitivity (lipidic tissue, 80.49%) obtains highest improvement (+5%), while the calcified tissue, starting with a quite good sensitivity value (92.20%) remains at the same value. This fact experimentally confirms that

the design of the J^S contribution in the *J* function proposed in Eq. 1 is effective.

The improvements achieved by the *BI* method are poor and unpredictable. This behavior can be justified by the naïve formulation of data inclusion process. The *LDS semi-supervised* inclusion method does not improve with respect to *IvtD* case. The only significant improvement is in the lipidic class sensitivity. This behavior could be explained by the fact that LDS looks for a minimum density path to cluster data. Since the lipidic plaque is under-represented in the training set, the improvement in the corresponding sensitivity is expected. However, this improvement comes at the cost of hindering calcium and fibrotic performance. These results suggest that a pure *semi-supervised* approach may be not enough for the goal of fusing data sets in plaque characterization.

The proposed *pSFFS* methods results in an improvement of the overall accuracy in discriminating in-vivo plaques of around 13% with respect to the *IvtD* case. Furthermore, each classification performance parameter exhibits a significant improvement. Although the in-vivo data set can not be assumed as a validated ground truth, the significant improvement can be considered as a qualitative result demonstrating the effectiveness in using the proposed approach in in-vivo plaque characterization problems. The achieved improvement is clearly due to the inclusion of selected in-vivo data into the in-vitro data set.

We demonstrate that the high accuracy achieved by a classifier trained with in-vitro data (*IvtD*) is different if it is used to test in-vitro (89%) or in-vivo (74%) data. The result, though qualitative, confirms that the hypothesis of assuming the difference between in-vivo and in-vitro as negligible, is incorrect.

Conclusions

In this paper we presented an extension of the SFFS algorithm with the aim of fusing in-vivo and in-vitro data to create an enhanced IVUS data set for plaque characterization. The proposed *pSFFS* method accomplishes the proposed goal and outperforms all the algorithms considered in the comparison. Experimental results show that the enhanced classifier maintains (actually improves) the discriminative power on in-vitro data, achieving an overall accuracy of 91.59%.

Note that, as each other plaque characterization methodology proposed in recent years, this result is achieved by characterizing plaques in validated post-mortem cases. The results in classifying in-vivo data by means of the enhanced classifier suggests that it could be effectively used in clinical plaque characterization problems; Furthermore, it demonstrates that a classifier trained and validated solely with in-vitro data does not exhibit the same discriminative power on in-vivo cases.

A possible future work could comprise the investigation and comparison using alternative J functions. Finally, though the method is presented on only three plaque types, the achieved results are of general validity.

Acknowledgments This work was supported in part by a research grant from projects TIN2006-15308-C02, TIN2009-14404-C02, FIS-PI061290, FIS-PI060957, FIS-PI070454, CONSOLIDER INGENIO 2010 (CSD2007-00018).

References

- Shah PK (2003) Mechanism of plaque vulnerability and rupture. *JACC* 41(1):15–22
- Burke AP, Farb A, Malcom GT, Liang Y, Smialek J, Virmani R (1997) Coronary risk factors and plaque morphology in men with coronary disease who died suddenly. *New Engl J Med* 336(18):1276–1281
- Fuster V, Moreno PR, Fayad ZA, Corti R, Badimon JJ (2005) Atherothrombosis and high-risk plaque. *JACC* 46(6):937–954
- Ehara S, Kobayashi Y, Yoshiyama M, Shimada K, Shimada Y, Fukuda D, Nakamura Y, Yamashita H, Yamagishi H, Takeuchi K, Naruko T, Haze K, Becker AE, Yoshikawa J, Ueda M (2004) Spotty calcification typifies the culprit plaque in patients with acute myocardial infarction: an intravascular ultrasound study. *Circulation* 110:3424–3429
- Willerson JT, Wellens HJJ, Cohn JN, Holmes DR (2007) Atherosclerotic vulnerable plaques: pathophysiology, detection, and treatment. *Cardiovasc Med*, Third Ed 10: 621–639
- Davies MJ, Thomas AC (1995) Plaque fissuring—the cause of acute myocardial infarction, sudden ischaemic death, and crescendo angina. *Br Heart J* 53(4):363–373
- Zhang X, McKay CR, Sonka M (1998) Tissue characterization in intravascular ultrasound images. *TMI* 17(6): 889–899
- Caballero KL, Barajas J, Pujol O, Salvatella N, Radeva P (2006) In-vivo ivus tissue classification: a comparison between rf signal analysis and reconstructed image. *Prog Pattern Recognit Image Anal* 4225/2006:137–146
- Caballero KL, Barajas J, Pujol O, Rodríguez O, Radeva P (2007) Using reconstructed ivus images for coronary plaque classification. In: Proceedings of the 29th annual international conference of the IEEE EMBS
- Moore M, Spencer T, Salter D, Kearney P, Shaw T, Starkey I, Fitzgerald P, Erbel R, Lange A, McDicken N, Sutherland G, Fox K (1998) Characterisation of coronary atherosclerotic morphology by spectral analysis of radio-frequency signal: in vitro intravascular ultrasound study with histological and radiological validation. *Heart* 79(5): 459–467
- Nair A, Kuban BD, Tuzcu EM, Schoenhagen P, Nissen SE, Vince DG (2002) Coronary plaque classification with intravascular ultrasound radiofrequency data analysis. *Circulation* 106:2200–2206
- Nair A, Kuban BD, Obuchowski N, Vince GD (2001) Assessing spectral algorithms to predict atherosclerotic plaque composition with normalized and raw intravascular ultrasound data. *UMB* 27(10):1319–1331
- Katouzian A, Sathyanarayana S, Baseri B, Konofagou EE, Carlier SG (2008) Challenges in atherosclerotic plaque characterization with intravascular ultrasound (ivus): from data collection to classification. *TITB* 12(3):315–27
- Bedekar D (2003) Atherosclerotic plaque characterization by acoustic impedance analysis of intravascular ultrasound data. In: *IEEE ultrasonic symposium*, vol 1527
- Sathyanarayana S, Carlier S, Wenguan L, Thomas L (2009) Characterization of atherosclerotic plaque by spectral similarity of radiofrequency intravascular ultrasound signals. *EuroIntervention* 5:133–139
- Kawasaki M, Takatsu H, Noda T, Ito Y, Kunishima A, Arai M, Nishigaki K, Takemura G, Morita N, Minatoguchi S, Fujiwara H (2001) Noninvasive quantitative tissue characterization and two-dimensional color-coded map of human atherosclerotic lesions using ultrasound integrated backscatter. *JACC* 38(2):486–492
- Kawasaki M, Takatsu H, Noda T, Sano K, Ito Y, Hayakawa K, Tsuchiya K, Arai M, Nishigaki K, Takemura G, Minatoguchi S, Fujiwara T, Fujiwara H (2002) In vivo quantitative tissue characterization of human coronary arterial plaques by use of integrated backscatter intravascular ultrasound and comparison with angioscopic findings. *Circulation* 105:2487–2492
- Kawasaki M, Sano K, Okubo M, Yokoyama H, Ito Y, Murata I, Tsuchiya K, Minatoguchi S, Zhou X, Fujita H, Fujiwara H (2005) Volumetric quantitative analysis of tissue characteristics of coronary plaques after statin therapy using three-dimensional integrated backscatter intravascular ultrasound. *JACC* 45(12):1946–1953
- Korte CD, Steen AD, Cespedes E, Pasterkamp G, Carlier SG, Mastik F, Schoneveld AH, Serruys PW, Bom N (2000) Characterization of plaque components and vulnerability with intravascular ultrasound elastography. *Circulation* 102:617–623
- Korte CD, Sierevogel MJ, Mastik F, Strijder C, Schaar JA, Velema E, Pasterkamp G, Serruys PW, Steen AVD (2002) Identification of atherosclerotic plaque components with intravascular ultrasound elastography in vivo: a yucatan pig study. *Circulation* 105(14):1627–1630
- Schaar JA, Regar E, Mastik F, McFadden EP, Saia F, Disco C, deKorte CL, Feyter PJ, der Steen AV, Serruys PW (2004) Characterizing vulnerable plaque features with intravascular elastography. *Circulation* 109:2716–2719

22. Murashige A, Hiro T, Fujii T, Imoto K, Murata T, Fukumoto Y, Matsuzaki M (2005) Detection of lipid-laden atherosclerotic plaque by wavelet analysis of radiofrequency intravascular ultrasound signals: in vitro validation and preliminary in vivo application. *JACC* 45(12):1954–1960
23. Pudil P, Ferri FJ, Novovicova J, Kittler J (1994) Floating search methods for feature selection with nonmonotonic criterion functions. In: Proceedings of the 12th IAPR international conference on pattern recognition, vol 2, pp 279–283
24. Ciompi F (2008) Ecoc-based plaque classification using in-vivo and ex-vivo intravascular ultrasound data. Master thesis
25. Dietterich TG, Bakiri G (1995) Solving multiclass learning problems via error-correcting output codes. *J Artif Intell Res* 2:263–286
26. Allwein EL, Schapire RE, Singer Y (2000) Reducing multiclass to binary: a unifying approach for margin classifiers. In: Proceedings of the seventeenth international conference on machine learning, pp 9–16
27. Schapire R (2001) The boosting approach to machine learning: an overview. MSRI workshop on nonlinear estimation and classification
28. Gonzalez RC, Woods RE (2001) Digital image processing, 2nd edn. Prentice Hall, Upper Saddle River
29. Bovik AC, Clark M, Geisler WS (1990) Multichannel texture analysis using localized spatial filters. *TPAMI* 12(1):55–73
30. Ojala T, Pietikäinen M, Mäenpää T (2002) Multiresolution gray-scale and rotation invariant texture classification with local binary patterns. *TPAMI* 24(7):971–987
31. Pujol O, Vitria J, Radeva P (2006) Discriminant ecoc: a heuristic method for application dependent design of error correcting output codes. *TPAMI* 28(6):1007–1012
32. Escalera S, Pujol O, Mauri J, Radeva P (2008) Ivus tissue characterization with sub-class error-correcting output codes. *J Signal Process Syst* 55:35–47
33. Rifkin R, Klautau A (2004) In defense of one-vs-all classification. *J Mach Learn Res* 5:101–141
34. Djouadi A, Snorrason O, Garber FD (1990) The quality of training sample estimates of the bhattacharyya coefficient. *PAMI* 12(1):92–97. doi:[10.1109/34.41388](https://doi.org/10.1109/34.41388)
35. Borg I, Groenen P (2005) Modern multidimensional scaling: theory and applications, 2nd edn. Springer, New York
36. Chapelle O, Zien A (2004) Semi-supervised classification by low density separation. In: Proceeding of the tenth international workshop on artificial intelligence and statistics, pp 57–64
37. Wang J, Shen Z, Pan W (2007) On transductive support vector machines. *Predict Discov*